^{13}C-^{1}H NMR Relaxation and Fluorescence Anisotropy Decay Study of Tyrosine Dynamics in Motilin

Peter Damberg,* Jüri Jarvet,* Peter Allard,† Ülo Mets,‡ Rudolf Rigler,‡ and Astrid Gräslund*

*Department of Biochemistry and Biophysics, Arrhenius Laboratories, Stockholm University, S-106 91 Stockholm, Sweden; †Structural Biochemistry, Department of Biotechnology, Stockholm Center for Physics, Astronomy, and Biotechnology, The Royal Institute of Technology, S-106 91 Stockholm, Sweden; and ‡Department of Medical Biophysics, Karolinska Institute, S-171 77 Stockholm, Sweden

ABSTRACT Tyrosine ring dynamics of the gastrointestinal hormone motilin was studied using two independent physical methods: fluorescence polarization anisotropy decay and NMR relaxation. Motilin, a 22-residue peptide, was selectively ^{13}C labeled in the ring ϵ-carbons of the single tyrosine residue. To eliminate effects of differences in peptide concentration, the same motilin sample was used in both experiments. NMR relaxation rates of the tyrosine ring C^{ϵ}-H^{ϵ} vectors, measured at four magnetic field strengths (9.4, 11.7, 14.1, and 18.8 Tesla) were used to map the spectral density function. When the data were analyzed using dynamic models with the same number of components, the dynamic parameters from NMR and fluorescence are in excellent agreement. However, the estimated rotational correlation times depend on the choice of dynamic model. The correlation times estimated from the two-component model-free approach and the three-component models were significantly different (1.7 ns and 2.2 ns, respectively). Various earlier studies of protein dynamics by NMR and fluorescence were compared. The rotational correlation times estimated by NMR for samples with high protein concentration were on average 18% longer for folded monomeric proteins than the corresponding times estimated by fluorescence polarization anisotropy decay, after correction for differences in viscosity due to temperature and D_2O/H_2O ratio.

INTRODUCTION

NMR relaxation and fluorescence polarization anisotropy decay (FAD) are two important experimental methods to study the dynamics of biomolecules. The results from the two methods on protein dynamics have been compared for a number of proteins listed in Table 1. In several cases the global rotational correlation time deviates significantly between the two methods. In most cases the correlation time observed by fluorescence is shorter than the correlation time observed by NMR. The details of this table will be discussed later. A fraction of the observed discrepancies between the NMR data and the fluorescence data can be explained by the typical difference in concentration between NMR and fluorescence studies.

Because FAD and NMR relaxation are about the only two experimental approaches to detailed studies of molecular dynamics, it is important to try to reconcile the results and find out where the results from the two methods deviate from each other and become less reliable.

Motilin is a gastrointestinal peptide hormone with 22 amino acids, among them the single Tyr^7 fluorophore. In our previous study of motilin dynamics (Allard et al., 1995; Jarvet et al., 1996) we found that the overall rotational correlation time of motilin is ~5 ns at 20°C and 3 ns at 35°C in 30% hexafluoro-2-propanol (HFP), evaluated by spectral density mapping and with Leu^{10} α-carbon as the probe for the relaxation measurements. These results were significantly different from the value (2.2 ns at 20°C in 30% HFP) measured by FAD on the single Tyr residue of the peptide.

In the present study we have continued the studies of the motilin peptide and have looked into various possible sources of systematic errors for the dynamic information from NMR and FAD. Typical peptide concentrations lie in the millimolar range for NMR and in the micromolar range for FAD. Here we have used the same sample in both experiments to eliminate this source of error. In addition, we have placed the ^{13}C labels in the ϵ-positions of the tyrosine ring to probe the same region of the molecule in both the NMR and the FAD experiment. The observations show that it is possible to obtain very similar results reflecting spectral densities by fluorescence and NMR and suggest that different systematic errors may appear in the interpretation of the data when dynamic models are applied. In the course of the study we have also applied a new version of the spectral density mapping method, where only the most accurately and precisely determined relaxation rates measured at different magnetic fields are used for the determination of spectral densities.

THEORY

Chemical shift anisotropy and dipole-dipole mechanisms

For protonated aromatic ring carbons, both dipole-dipole (DD) and chemical shift anisotropy (CSA) mechanisms contribute to relaxation. The dipolar interaction constant is a function of distance and in the case of two half-spins I and

Submitted May 19, 2002, and accepted for publication June 5, 2002.

Address reprint requests to Dr. Astrid Gräslund, Department of Biochemistry and Biophysics, Arrhenius Laboratories, Stockholm University, S-106 91 Stockholm, Sweden. Tel.: 46-8-162450; Fax: 46-8-155597; E-mail: astrid@dbb.su.se.

0006-3495/02/11/2812/14 $2.00

TABLE 1 Comparison of rotational correlation times τ and corresponding hydrodynamic volumes V_h estimated from NMR and FAD data

Protein	Number of residues	Molecular mass (kDa)	τ (ns)		V_h (nm)^3			
			FAD	NMR	Calculated	FAD†	NMR†	V_h^{NMR}/V_h^{FAD}
Zinc finger Xfin-31	25	3.0	1.1‡	1.4‡	7.9	5.5	6.4	1.25
Barstar	89	10.2	4.1§	5.2¶	21.2	18.7	26.1	1.43
Calbindin D_{9k} (apo)	75	8.6	3.7‖	4.1**	18.4	16.9	17.8	1.15
Calbindin D_{9k} Ca^{2+}	75	8.6	4.2‖	4.3††	18.4	19.2	18.1	1.05
Thioredoxin (reduced)	108	11.7	5.7‡‡	10.1‡‡	23.7	23.1	30.1	1.46
Thioredoxin (oxidized)	108	11.7	6.0‡‡	10.5‡‡	23.7	24.1	31.3	1.45
Defunct domain of CaVP	86	9.9	6.8§§	7.1§§	20.6	31.1	31.0	1.02
Δ^5-3-Ketosteroid isomerase	2*125 (dimer)	26.8	18.0¶¶	17.9‖‖	48.3	72.5	70.2	0.99
Carp parvalbumin	108	11.7	4.7***	4.6***	23.7	23.7	21.8	0.97
Azurin	129	14.7	6.5†††	4.7‡‡‡	28.7	26.3	26.8	1.10
Lysozyme	129	14.3	4.4§§§	5.7¶¶¶	28.1	22.2	27.6	1.43
Protein G	56	6.5	3.1‖‖‖	4.2****	14.6	12.6	16.6	1.32
Motilin	22	2.7	0.7††††	1.4‡‡‡‡	7.3	2.9	6.8	2.33
Staphylococcal nuclease	149	18.0	12.7§§§§	9.1¶¶¶¶	34.2	51.4	50.0	0.97
Mellitin (random coil)	26	2.9	1.0‖‖‖‖	1.3‖‖‖‖	7.6	4.1	4.3	1.05
Mellitin	4*26 (tetramer)	11.4	2.5‖‖‖‖	4.2‖‖‖‖	23.2	10.1	14.0	1.38
Ribonuclease T1	104	11.0	3.5, 6.0*****	4.2†††††	22.5	18.9, 30.4	29.3	1.55, 0.96

*The hydrodynamic volume was calculated from the molecular mass, assuming spherical shape and a density of the protein of 1.33 g/cm^3 with a monomolecular hydration layer of 2.8 Å.

†The hydrodynamic volume was calculated from the rotational correlation time using the Stokes-Einstein relation $V_h = \tau_m k_B T/\eta$ where the viscosity η was estimated from the temperature-dependent viscosities of H_2O and D_2O.

Values were obtained from the following references: ‡Palmer et al., 1993; §Swaminathan et al., 1994; ¶Sahu et al., 2000; ‖Rigler et al., 1990; **Akke et al., 1993; ††Kördel et al., 1992; ‡‡Kemple et al., 1994; §§Théret et al., 2001; ¶¶Wu et al.; ‖‖Zhao et al., 1996; ***Moncrieffe et al., 2000; †††Kroes et al., 1998; ‡‡‡Kalverda et al., 1999; §§§Nishimoto et al., 1998; ¶¶¶Buck et al., 1995; ‖‖‖Tcherkasskaya et al., 2000; ****Seewald et al., 2000; ††††Backlund et al., 1995; ‡‡‡‡Jarvet et al., 1996; §§§§Wong and Eftink, 1998; ¶¶¶¶Kay et al., 1989; ‖‖‖‖Kemple et al., 1997; *****Chen et al., 1987; and James, 1985; †††††Fushman et al., 1994.

S, it has the following value (Peng and Wagner, 1992; Allard et al., 1998):

$$A_{IS}^{DD} = 3\frac{\mu_0}{4\pi}\frac{h}{2\pi}\frac{\gamma_I\gamma_S}{r_{IS}^3}, \quad (1)$$

where $\mu_0/4\pi$ is the conversion factor to SI system units, h is Planck's constant, and r_{IS} is the internuclear distance between spins I and S. The CSA interaction constant is a function of the polarizing magnetic field B_0:

$$A_S^{CSA} = -\Delta\sigma\gamma_S B_0, \quad (2)$$

where $\Delta\sigma = \sigma_\parallel - \sigma_\perp$ is the difference between the parallel and orthogonal components of an axially symmetric CSA tensor.

A third possible relaxation mechanism is cross-correlation between the mentioned mechanisms. The interaction constant is a product of DD and CSA interaction constants and depends also on the angle between the CSA tensor and the internuclear vector. Although one of the interactions may cause a negligible auto-relaxation rate, the product of the two interaction constants may still be large. Special measures may have to be taken to suppress this interaction, as will be discussed in the Materials and Methods section dealing with the pulse sequences (Palmer et al., 1992).

The CSA mechanism interaction constant has been determined for the ^{13}C-H vector on the tyrosine ring by experiments that yield the field dependence of longitudinal relaxation (Damberg et al., 1999). The CSA parameter $\Delta\sigma_{eff}$ was -156 ppm, close to the value reported from solid-state NMR studies (Frydman et al., 1992). The dipolar interaction constant was calculated with a C-H distance taken from a neutron diffraction study (Frey et al., 1973). With a correction for thermal vibrations, the effective length of the C-H vector is 1.09 Å, which is the fixed value used in the present study.

Spectral density function

To analyze FAD data and NMR relaxation rates in terms of dynamics parameters, a model of mobility has to be selected. The isotropic rotation model, described by a single correlation time τ_m, is inadequate for describing the dynamics of the tyrosine ring in the peptide. A widely used model in NMR is based on the so-called model-free approach (Lipari and Szabo, 1982). The model may be considered as a description of dynamics assuming two independent motional processes with time constants τ_m and τ_e and a generalized order parameter S^2.

In fluorescence a corresponding approximation is to analyze the FAD with two exponential components with time constants τ_1 and τ_2 and amplitudes A_1 and A_2. One can directly compare the parameters obtained by the two methods.

The expression for the spectral density obtained from the model-free approach is the sum of two Lorentzian components:

$$J(\omega) = \frac{2}{5}\left[\frac{S^2\tau_m}{1 + (\omega\tau_m)^2} + \frac{(1 - S^2)\tau_{eff}}{1 + (\omega\tau_{eff})^2}\right] \quad (3)$$

The FAD function can be expressed as follows:

$$C(t) = A_1 \exp(-t/\tau_1) + A_2 \exp(-t/\tau_2) \quad (4)$$

In both cases, the longer time constant (τ_m or τ_1) is assigned to the overall rotational correlation time. The correlation time for local motion in the model-free approach is τ_e, related to τ_{eff} as follows: $\tau_{eff}^{-1} = \tau_m^{-1} + \tau_e^{-1}$. The ratio $A_1/(A_1 + A_2)$ of the fluorescence anisotropy amplitudes corresponds to an order parameter. At the outset one would expect the same time constants to be observed in the NMR and FAD experiments, but not necessarily with the same relative amplitudes because of the different orientations of the interaction vectors relative to the tyrosine ring.

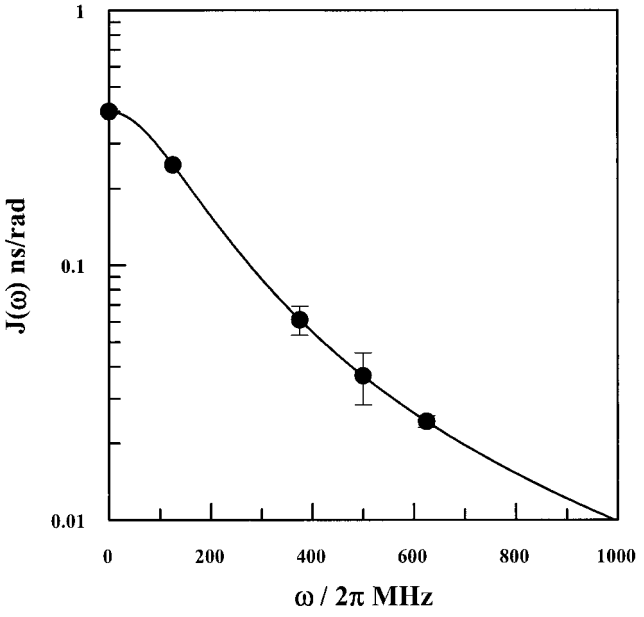

FIGURE 1 Error propagation for SDM. The solid line corresponds to isotropic rotation with a correlation time of 1.0 ns. Synthetic relaxation data were calculated using this spectral density function, and spectral density values were calculated using Eq. 1. Spectral density points are shown along with error bars calculated assuming a 1% error in relaxation rates. Relaxation caused by other protons, ρ_{HH}, was fixed to 1 s^{-1}.

Spectral density mapping

To carry out full spectral density mapping as originally suggested by Peng and Wagner (1992), six dipolar relaxation rates have to be measured: the carbon longitudinal relaxation rate $R_C(C_z)$, the carbon in-phase transverse relaxation rate $R_C(C_x)$, the carbon anti-phase transverse relaxation rate $R_{CH}(2H_zC_x)$, the relaxation rate of longitudinal two-spin order $R_{CH}(2H_zC_z)$, the proton longitudinal relaxation rate $R_H(H_z)$, and the heteronuclear cross-relaxation rate σ_{CH}. The proton relaxation rate ρ_{HH} accounts for relaxation caused by other protons. The relation between measured relaxation rates and spectral densities is expressed by the matrix:

$$\begin{bmatrix} R_C(C_z) \\ R_C(C_x) \\ R_{CH}(2H_zC_x) \\ R_{CH}(2H_zC_z) \\ R_H(H_z) \\ \sigma_{CH} \end{bmatrix} = \begin{bmatrix} 0 & 3d + c & d & 0 & 6d & 0 \\ \frac{6d + 2c}{3} & \frac{3d + c}{2} & \frac{d}{2} & 3d & 3d & 0 \\ \frac{6d + 2c}{3} & \frac{3d + c}{2} & \frac{d}{2} & 0 & 3d & 1 \\ 0 & 3d + c & 0 & 3d & 0 & 1 \\ 0 & 0 & d & 3d & 6d & 1 \\ 0 & 0 & -d & 0 & 6d & 0 \end{bmatrix} \times \begin{bmatrix} J(0) \\ J(\omega_C) \\ J(\omega_H - \omega_C) \\ J(\omega_H) \\ J(\omega_H + \omega_C) \\ \rho_{HH} \end{bmatrix} \quad (5)$$

For simplicity, the interaction coefficients d and c are introduced, where $d = [(1/6)A_{CH}^{DD}]^2$ and $c = [(1/\sqrt{3})A_{CH}^{CSA}]^2$. The values of the constants used in the expressions are $\gamma_H = 26.753 \times 10^{10}$ rad s^{-1} T^{-1}, $\gamma_C = 6.728 \times 10^{10}$ rad s^{-1} T^{-1}, and $h = 6.62 \times 10^{-34}$ J s. For a C-H bond length $r_{CH} = 1.09$ Å, one obtains $d = 5.37 \times 10^9$ rad^2 s^{-2} and $c = 3.22 \times 10^9$ rad^2 s^{-2} for $\Delta\sigma = -156$ ppm at the magnetic field 9.36 T.

The inverse of Eq. 5 describes how the spectral densities are calculated from the measured relaxation rates. Errors in the measured rates propagate unequally into the determined spectral densities. Fig. 1 illustrates this for the simple case of isotropic rotation with a correlation time $\tau_m = 1$ ns and a 1% error in all of the measured rates. The propagated relative error is largest for $J(\omega_H)$ (23%). In the simplified version of spectral density mapping (SDM) to be described we will exclude this value from the spectral density map.

Simplified SDM

When the spectral density at the proton frequency, $J(\omega_H)$, is not included in the SDM, one rate can also be omitted from the measurements. For reasons described below, we excluded the carbon anti-phase transverse relaxation rate from the relations. The spectral density at the proton Larmor frequency $J(\omega_H)$ may now be approximated by $J(\omega_H) = [J(\omega_H - \omega_C) + J(\omega_H + \omega_C)]/2$. The six equations described by Eq. 5 may then be simplified to five equations. The simplified spectral density matrix is obtained as follows:

$$\begin{bmatrix} R_C(C_z) \\ R_C(C_x) \\ R_{CH}(2H_zC_z) \\ R_H(H_z) \\ \sigma_{CH} \end{bmatrix} = \begin{bmatrix} 0 & 3d+c & d & 6d & 0 \\ \frac{6d+2c}{3} & \frac{3d+c}{2} & 2d & \frac{9d}{2} & 0 \\ 0 & 3d+c & \frac{3d}{2} & \frac{3d}{2} & 1 \\ 0 & 0 & \frac{5d}{2} & \frac{15d}{2} & 1 \\ 0 & 0 & -d & 6d & 0 \end{bmatrix} \times \begin{bmatrix} J(0) \\ J(\omega_C) \\ J(\omega_H - \omega_C) \\ J(\omega_H + \omega_C) \\ \rho_{HH} \end{bmatrix} \quad (6)$$

By inverting the matrix of Eq. 6, the following expression is obtained for spectral densities:

$$\begin{bmatrix} J(0) \\ J(\omega_C) \\ J(\omega_H - \omega_C) \\ J(\omega_H + \omega_C) \\ \rho_{HH} \end{bmatrix} = \begin{bmatrix} \frac{-45}{32(3d+c)} & \frac{3}{2(3d+c)} & \frac{21}{32(3d+c)} & \frac{-21}{32(3d+c)} & \frac{15}{16(3d+c)} \\ \frac{1}{6d+2c} & 0 & \frac{1}{6d+2c} & \frac{-1}{6d+2c} & 0 \\ \frac{1}{4d} & 0 & \frac{-1}{4d} & \frac{1}{4d} & \frac{-1}{2d} \\ \frac{1}{24d} & 0 & \frac{-1}{24d} & \frac{1}{24d} & \frac{1}{12d} \\ -\frac{15}{16} & 0 & \frac{15}{16} & \frac{1}{16} & \frac{5}{8} \end{bmatrix} \times \begin{bmatrix} R_C(C_z) \\ R_C(C_x) \\ R_{CH}(2H_zC_z) \\ R_H(H_z) \\ \sigma_{CH} \end{bmatrix} \quad (7)$$

Notice that there is a significant difference between this equation and those used for reduced SDM, often used when ^{15}N relaxation rates are measured. For reduced SDM, the ^{15}N longitudinal and transverse relaxation and the steady-state $\{^1H\}$-^{15}N nuclear Overhauser enhancement (NOE) are measured, and from these rates $J(0)$, $J(\omega_N)$, and $J(0.870\omega_H)$ are evaluated (Farrow et al., 1995; Ishima and Nagayama, 1995).

Internuclear distance

The interaction constants determine the area under the spectral density function. The dipolar interaction depends on the inverse of the sixth power of the internuclear distance of the CH bond in the tyrosine ring. Therefore it is important that an accurate distance value is used when relaxation rates are analyzed. The value obtained from neutron diffraction studies (1.08 Å (Frey et al., 1973)) has to be corrected for rapid thermal motions (internal motions much faster than the Larmor frequency in NMR). The resulting value of 1.09 Å is generally used, also in the present study.

The C-H bond lengths for the two distinct ions in calcium formate were determined to be 1.130 and 1.126 Å by dipolar switching-angle sample spinning NMR in the solid state without considering vibrations (Terao et al., 1986). Anisotropic out-of-plane vibrations (librations) with an amplitude of 12–15° could account for this increase of the effective bond length (Nakai et al., 1989). For the C^α-H^α bond in proteins it was observed already in the pioneering relaxation experiments on alumichrome (Llinas et al., 1977) and on lysozyme (Dill and Allerhand, 1979) that longer effective distances of 1.11 Å and 1.15 Å, respectively, will improve the fit to the experimentally measured ^{13}C relaxation rates. The average bond length of C^α-H^α was recently determined with high accuracy for ubiquitin in a dilute liquid-crystalline phase (Ottiger and Bax, 1998) and found to be 1.117 ± 0.007 Å. This is considerably longer than the equilibrium or average internuclear distances derived from ab initio calcu-

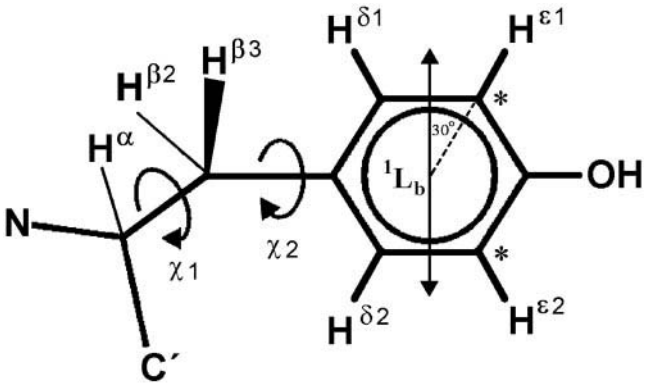

FIGURE 2 The tyrosine residue with atom definitions according to IUPAC recommendations (Markley et al., 1998). The fluorescence transition moment for the ^1L_b transition makes an ~30° angle with the NMR dipolar C-H vector, ^{13}C-labeled (*) in $\epsilon 1$, $\epsilon 2$ for the present study.

lations, neutron diffraction, or microwave spectroscopy. This longer distance value is in excellent agreement with the effective internuclear distance determined by treating the internuclear distance as an adjustable parameter when fitting the model-free model to spectral density data points, obtained by SDM for the C^α-H^α bond of Leu^{10} in motilin (Jarvet et al., 1996). The longer effective bond length has also been reproduced by quantum chemical methods by taking vibrations into account (Case, 1999).

The effective bond lengths in L-tyrosine-HCl were recently determined by solid-state NMR (De Paul et al., 2000). The effective bond lengths of the two nonequivalent carbon-proton pairs in ortho position were found to be 1.12 ± 0.02 Å and 1.15 ± 0.05 Å, respectively. Those distances are considerably longer than the distances estimated by neutron diffraction (Frey et al., 1973). An increase of the effective internuclear distance from 1.09 to 1.12 Å corresponds to an 18% decrease of the evaluated spectral densities. How the internuclear distance parameter affects the evaluated dynamic parameters will be discussed later. It is important to note that bending vibrations (librations) lead to an increase of the effective internuclear distance. Stretching vibrations in the harmonic approximation result in a decrease in the effective internuclear distance (Lipari and Szabo, 1982).

MATERIALS AND METHODS

Sample

The motilin sample is described in detail in Damberg et al. (1999). The peptide contained two specific ^{13}C labels in the ϵ-positions of the single tyrosine residue (Fig. 2). The peptide was 5 mM in 30% hexafluoroisopropanol-d/10% D_2O/60% H_2O. All experiments were performed at 35°C ± 0.1°C. The temperature was measured with a thermocouple thermometer directly inserted into the NMR sample tube.

NMR measurements

NMR relaxation rates were measured with Varian Inova spectrometers equipped with inverse detection probe heads, and sensitivity-enhanced pulse sequences were used. Delay lists for relaxation experiments consisted of 10 linearly spaced delays starting from zero and covered up to two time constants. Good solvent suppression was achieved, and no baseline corrections were needed.

Translational diffusion coefficients were measured by the longitudinal eddy-current delay pulsed field gradient pulse sequence (Gibbs and Johnson, 1991). The gradient strength was calibrated and the attenuation curves were evaluated as suggested in Damberg et al. (2001). The gradient pulses had a duration of 5 ms, and the strength of the gradient pulses was varied between 0 and 0.3 T/m in 30 steps. The spacing between the diffusion encoding gradient pulses was 0.2 s. The solvent signal was suppressed by 2 s of presaturation during the 5-s recycling delay.

The NMR longitudinal relaxation rates $R_C(C_z)$ and $R_{CH}(2H_zC_z)$, and the steady-state $\{^1H\}$-^{13}C NOE were measured as described previously (Dayie and Wagner, 1994).

Transverse inphase relaxation rate $R_C(C_x)$ and anti-phase rate $R_{CH}(2H_zC_x)$

The ^{13}C transverse relaxation rate $R_C(C_x)$ was measured using an on-resonance spin lock. Proton inversion pulses every 500 μs during the relaxation delay were used to suppress the CSA-DD cross-correlation. The anti-phase rate $R_{CH}(2H_zC_x)$ was first measured by the previously described pulse sequence (Dayie and Wagner, 1994). A decay curve that was clearly not a single-exponential decay was obtained. An initial approximation of the apparent decay rate was found to be 19 s^{-1}, which is twice as fast as the expected rate. The method of Loria et al. (1999), i.e. an ordinary spin echo with a long delay between refocusing pulses, is supposed to yield a single-exponential decay curve. Its rate should be the average of the anti-phase and in-phase relaxation rates. This method indeed yielded a single-exponential decay curve, but the back-calculated anti-phase rate was still too fast by a factor of two. Others have also reported serious problems in measuring the anti-phase relaxation rates accurately (Markus et al., 1996). In the present case, the high rate may be related to the fact that both ϵ-carbons, separated by only one carbon atom in the tyrosine ring, are labeled by ^{13}C. Because of the problems with the anti-phase rate, we decided to exclude it from the SDM and used the simplified version based on Eqs. 6 and 7.

Proton longitudinal relaxation rate $R_H(H_z)$

An important experimental development for SDM is the pulse sequence for measuring proton auto-relaxation rate without interference from other protons. The pulse sequence is previously illustrated by Fig. 2 in the study by Damberg et al. (1999). In this experiment, cross-relaxation from other protons (spin diffusion) is eliminated by performing selective pulses in accordance with the suggestions by Norwood (1996, 1997). The experiments are performed in an add/subtract manner, with selective proton inversion in the middle of the of the relaxation delay. With this technique one observes a single-exponential decay with a time constant of ^1H T_1.

Fluorescence measurements

Time-resolved fluorescence experiments were performed using the time-correlated single-photon counting method. A laser system, consisting of a mode-locked argon ion laser pumping a cavity-dumped rhodamine 6G dye laser, including frequency doubling, was used for excitation at 286 nm. Such a long wavelength was chosen to have a sufficiently low absorbance of the tyrosine fluorophore, because, to measure under identical conditions

with the NMR sample, a high concentration (5 mM) of motilin was used. The sample temperature was controlled with a thermostated water bath. The temperature was measured with a thermocouple thermometer, directly inserted into the sample, and was adjusted to 35°C ± 0.1°C in all experiments.

Fluorescence emission data were collected in four different ways, alternating for 20 s each: laser light (for the response function), dark current, and perpendicular and parallel polarized fluorescence components, as previously described (Rigler et al., 1985; MacKerell et al., 1987). This cycle was repeated 10 times, resulting in 200 s of data collection for each signal. The data were analyzed in two steps as described previously (Kawato et al., 1977; Kouyama et al., 1989). First the isotropic fluorescence decay $S(t) = I_{\parallel} + 2I_{\perp}$ was fitted, using deconvolution with the measured response function. In the second step the fluorescence decay parameters were fixed, and the difference $D(t) = I_{\parallel} - I_{\perp}$ of the parallel and perpendicular fluorescence components was fitted, again using deconvolution. The deconvoluted theoretical fit function for this difference is $d(t) = r(t)s(t)$, where $r(t)$ is FAD and $s(t)$ is isotropic fluorescence decay, both corresponding to delta function excitation. For visual display of the fitting results, the fluorescence polarization anisotropy decay curves were calculated also directly from the experimental data as $(I_{\parallel} - I_{\perp})/(I_{\parallel} + 2I_{\perp})$. The rotational correlation times were evaluated under the assumption that each rotational component is associated with all fluorescence decay components.

RESULTS

NMR relaxation rate measurements

NMR relaxation rates of the selectively isotope labeled $^{13}C^{\epsilon 1}$-H and $^{13}C^{\epsilon 2}$-H vectors in the aromatic ring of tyrosine in the motilin peptide were measured at four magnetic field strengths of 9.36, 11.74, 14.09, and 18.79 T, corresponding to proton frequencies of 400, 500, 600, and 800 MHz, respectively. The relaxation rates needed for full SDM are the carbon longitudinal relaxation rate $R_C(C_z)$, the carbon in-phase transverse relaxation rate $R_C(C_x)$, the relaxation rate of longitudinal two-spin order $R_{CH}(2H_zC_z)$, the relaxation rate of carbon anti-phase coherence $R_{CH}(H_zC_x)$, and the proton longitudinal relaxation rate $R_H(H_z)$. The cross-relaxation rate σ_{CH} between proton and carbon was calculated from $R_C(C_z)$ and the steady-state $\{^1H\}$-^{13}C NOE using the relation:

$$\mathrm{NOE} = 1 + \frac{\gamma_H \sigma_{CH}}{\gamma_C R_C(C_z)} \tag{8}$$

The pulse sequences were based on those originally described in Dayie and Wagner (1994), except for the proton longitudinal relaxation rate. The accuracy of the measurement of ^1H T_1 is significantly increased by minimizing the interference from other protons (Damberg et al., 1999). This was achieved by a pulse sequence described in Materials and Methods.

The measured relaxation curves for the motilin peptide, 5 mM in concentration and in 30% HFP at 35°C were found to be single exponentials, except for the carbon anti-phase rate. This relaxation curve had the appearance of a double exponential, when it was measured using the original pulse sequence (Dayie and Wagner, 1994). When using the recently proposed improved pulse sequence (Loria et al., 1999), the curve became monoexponential in character, but still the rate was too fast to be consistent with the other rates in the full SDM. Despite various experimental efforts, including selective saturation of the protons in the δ-position, we were never confident that the anti-phase rate could be measured with any certainty. For this reason we decided to omit it from the SDM and instead use the simplified version (Eq. 7). Table 2 shows the six measured relaxation rates at the four magnetic fields.

TABLE 2 Relaxation rates of ε-carbon C-H vector of Tyr[7] in the peptide hormone motilin in 30% HFP at 35°C measured at four magnetic fields

B_0 (T)	$R_C(C_z)$ (s^{-1})	$R_{CH}(2H_zC_z)$ (s^{-1})	$R_H(H_z)$ (s^{-1})	σ_{CH} (s^{-1})	$R_C(C_x)$ (s^{-1})	$R_{CH}(2H_zC_x)$ (s^{-1})
9.39	4.15	4.78	2.81	0.54	6.90	17.6
11.74	3.49	4.44	2.27	0.50	7.13	19.2
14.09	3.05	3.98	2.08	0.42	7.53	19.0
18.79	2.58	3.45	1.60	0.35	8.65	
Uncertainty	0.024	0.072	0.11	0.020	0.018	

The experimental uncertainties in the relaxation rates (with the exception of the anti-phase rate that was omitted from the SDM) were estimated from the field dependences as described in the text.

The experimental errors in the relaxation rates (with the exception of the anti-phase rate that was omitted from the SDM) were estimated from the field dependences (Fig. 3). As the variation in the field strength is relatively small, a factor of only two, second-order polynomials were used to approximate the field dependences. The residuals were then used to estimate the measurement precision of the individual rates as the square root of the sum of squared residuals divided by the number of degrees of freedom. The results are included in Table 2. This approach is reasonable when the measurement precision is approximately equal at all fields. In practice, it has the advantage of including temperature miscalibration errors in the estimates of the imprecision.

The results presented in Fig. 3 show that the precision is generally very high in the measured rates. The least precise rate appears to be the proton longitudinal rate, which shows some very small deviations from a smooth second-order polynomial. The relaxation rates presented in Table 2 were used to calculate spectral densities according to Eq. 7, describing the simplified SDM method. The transverse anti-phase rates were not included in the calculation, for reasons stated above. The results in terms of spectral densities $J(0)$, $J(\omega_C)$, $J(\omega_H - \omega_C)$, and $J(\omega_H + \omega_C)$, measured at the four magnetic fields, are shown in Table 3. The values calculated for $J(\omega_H - \omega_C)$ are not included in Fig. 4. Apart from $J(\omega_H)$, this spectral density has the highest propagated error of the spectral densities (Fig. 1). The values of $J(0)$ evaluated from the results at the different magnetic fields showed some variations (Table 3), which will be further treated below. The other spectral densities seem to fall on a relatively

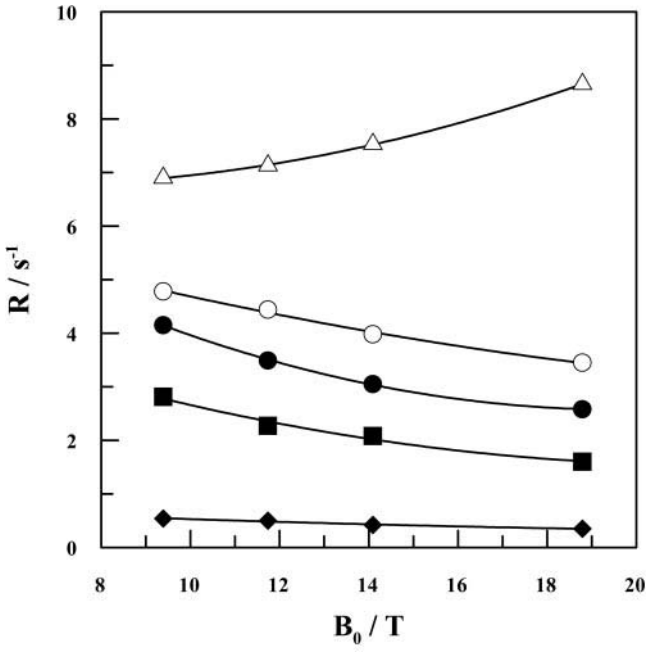

FIGURE 3 The relaxation rates as functions of magnetic field for the ^{13}C-labeled carbon-proton vector in ϵ-position of Tyr^7 in motilin in 30% (v/v) HFP at 35°C. The rates were measured at 9.39, 11.74, 14.09, and 18.79 T. The rates used for SDM are the carbon longitudinal relaxation rate $R_C(C_z)$ (●), the carbon in-phase transverse relaxation rate $R_C(C_x)$ (△), the relaxation rate of longitudinal two-spin order $R_{CH}(2H_zC_z)$ (○), the proton longitudinal relaxation rate $R_H(H_z)$ (■), and the heteronuclear cross-relaxation rate σ_{CH} (◆). Curves connecting the points represent the best fit of relaxation rates using second-order polynomials.

smooth curve. Error bars show the propagated spread of the calculated errors in the spectral densities from the estimated errors in the measured relaxation rates. These calculations were done assuming a fixed internuclear distance of 1.09 Å and an effective CSA of −156 ppm (Damberg et al., 1999).

The spectral densities are truly model-free parameters of the dynamics of a system. However, to obtain a more physical picture of the dynamics, a dynamic model has to be applied to the data. A simple three-parameter model, based on the assumption of two uncorrelated time constants, is provided by the model-free approach (Lipari and Szabo, 1982), as described in Eq. 3. The model was fitted to the spectral densities obtained by simplified SDM (SSDM), where the penalty function included weights according to the propagated error. The result is shown as the full curve in Fig. 4 *A*. The corresponding parameters (an order parameter and two correlation times) are shown in Table 4. In a dynamic interpretation, the longer rotational correlation time should correspond to the overall rotational motion of the molecule.

Exchange contributions to transverse relaxation

To search for possible evidence of the presence of a slow exchange process, the spin-lock field dependence of the carbon transverse auto-relaxation rate $R_C(C_x)$, i.e., $R_{1\rho}$, was studied. The $R_{1\rho}$ rate was measured at varying spin-lock power at 11.7 T. No systematic decrease in the rate with increasing spin-lock power was detectable (data not shown) in the range studied (20 Hz to 4.5 kHz). This is an indication of the absence of slow exchange in the kilohertz domain. At the highest spin-lock power it proved essential to use a long, i.e., 15 s, recovery time between transients to maintain the temperature at 35°C. With shorter recovery times, a false decrease in the relaxation rate was observed, concomitant with small phase and chemical shift changes probably caused by heating of both the sample and the RF-coil and/or amplifier power drop.

Contributions to the transverse auto-relaxation from conformational exchange faster than what can be observed in the spin-lock experiments can be detected as an increase of the apparent spectral density at zero frequency, $J(0)$, as a function of the static magnetic field B_0 (Peng and Wagner, 1995). They derive the following relation: $J(0)^{\text{apparent}} = J(0)^{\text{true}} + 3R_{ex}/(2c + 6d)$ in the fast exchange limit. Here c and d have the same meaning as above and the conformational exchange rate $R_{ex} = \Phi(\gamma_C B_0)^2$ for fast exchange and on-resonance spin-lock, where Φ is a proportionality constant.

If an exchange term is included in the spectral density model we obtain a slightly better fit of the spectral density function, but an F-test using the reduced χ^2 revealed that the improvement is not significant in the statistical sense. Fig. 5 shows the fitted spectral density functions with and without an assumed exchange term. Table 4 also includes the parameters obtained with the model-free approach when the exchange term is included in the fitting. In terms of parameters evaluated from the model-free approach for the two cases we found that the order parameter remained unchanged, whereas the rotational correlation time τ_m de-

TABLE 3 Spectral density values determined at four magnetic fields

B_0 T	$J(0)$ (ns rad^{-1})	$J(\omega_C)$ (ns rad^{-1})	$J(\omega_H - \omega_C)$ (ns rad^{-1})	$J(\omega_H + \omega_C)$ (ns rad^{-1})
9.39	0.326 ± 0.01	0.158 ± 0.05	0.0511 ± 0.01	0.0252 ± 0.002
11.74	0.362 ± 0.01	0.133 ± 0.05	0.0148 ± 0.01	0.0179 ± 0.002
14.09	0.369 ± 0.01	0.105 ± 0.05	0.0144 ± 0.01	0.0154 ± 0.002
18.79	0.374 ± 0.01	0.076 ± 0.05	0.0013 ± 0.01	0.0110 ± 0.002

Spectral densities were calculated from experimentally measured relaxation rates shown in Table 1 using the simplified spectral density method (Eq. 7) with $\Delta\sigma = 156$ ppm and $r_{CH} = 1.09$ Å.

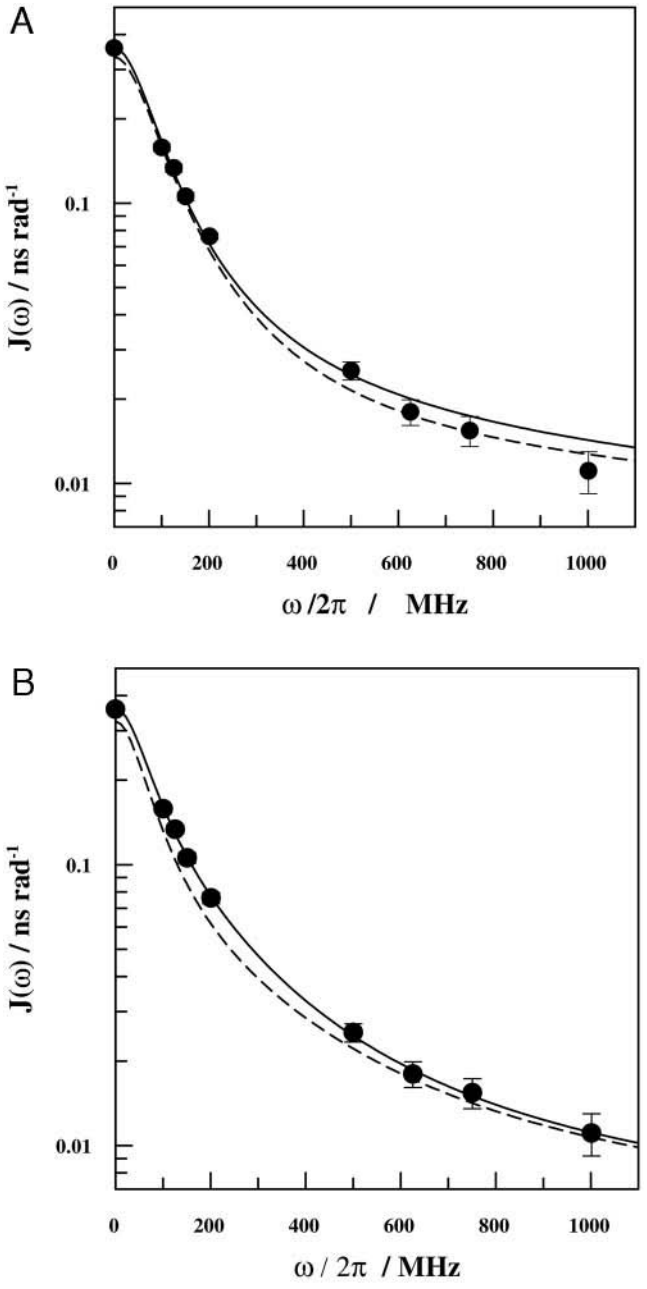

FIGURE 4 Spectral density values for the ^{13}C-labeled carbon-proton vector in ϵ-position of Tyr^7 in motilin at 35°C in 30% (v/v) HFP at different frequencies. The spectral density values were calculated from experimental relaxation rates measured at four magnetic fields using r_{CH} = 1.09 Å. The sampling frequencies are at zero frequency; at 100, 125, 150, and 200 MHz for $J(\omega_C)$; and at 500, 625, 750, and 1000 MHz for $J(\omega_H + \omega_C)$. The zero frequency spectral density is represented by the average of the four values estimated for each field, with the uncertainty estimated from the standard deviation of the four values. (*A*) The solid curve represents the best fit to a model-free spectral density function with τ_m = 1.7 ns, S^2 = 0.5, and τ_e = 60 ps. The dashed curve represents the fluorescence best fit to a two-component anisotropy decay function with corresponding model-free approach spectral density function parameters τ_m = 1.7 ns, S^2 = 0.47, and τ_e = 54 ps. (*B*) The two three-component models of molecular dynamics are shown together with the experimental spectral densities derived from NMR. The solid curve shows the spectral density function corresponding to the best-fitting three-component model (Eq. 10) to the NMR data with the following parameters: A_1 = 0.36, τ_1 = 2.1 ns, A_2 = 0.22, τ_2 = 0.59 ns, $A_3 = (1 - A_1 - A_2)$ = 0.42, and τ_3 = 0.037 ns. The dashed curve represents the three-component model obtained from fluorescence (Eq. 9) by fitting to the FAD data with the following parameters: A_1 = 0.33, τ_1 = 2.2 ns, A_2 = 0.17, τ_2 = 0.42 ns, $A_3 = (1 - A_1 - A_2)$ = 0.50, and τ_3 = 0.029 ns.

creased from 1.7 to 1.5 ns (Table 4). The question of exchange contribution to R_2 illustrates a remaining systematic error in the measurements, which leaves the spectral density at zero frequency with a significant uncertainty and mainly affects the estimated τ_m. This is despite the fact that extreme care was taken to ensure precision. It should be pointed out that these deliberations are not even possible to make, unless the relaxation is measured at several different fields. We would probably have needed measurements using at least one or two even lower fields to be able to conclude with any certainty about the absence or presence of conformational exchange contributions to the dephasing of transverse magnetization.

Fluorescence polarization anisotropy decay

The intrinsic fluorophore, the single tyrosine of the motilin peptide, was used to probe the rotational motion. The sample was identical in terms of concentration and other conditions to that of the NMR studies. The temperature was carefully calibrated and measured to coincide with the temperature used in the NMR studies. The isotropic fluorescence decay, which is a measure of the fluorescence lifetime, was fitted with a sum of three exponential components with amplitudes F_i and lifetimes φ_i. The best-fitting parameters were F_1 = 0.00292, φ_1 = 4.03 ns; F_2 = 0.0123, φ_2 = 1.33 ns; and F_3 = 0.00439, φ_3 = 0.28 ns.

The fluorescence anisotropy was evaluated by fitting a model with two exponential components (Eq. 4) to the data. The result is shown in Fig. 6, where also the residuals are included. The best-fitting values are A_1 = 0.13, τ_1 = 1.7 ns, A_2 = 0.14, and τ_2 = 0.054 ns. The sum of the amplitudes, A_1 and A_2, deviates from the theoretical value of 2/5, which is expected for parallel excitation and emission dipole moments. The amplitudes were rescaled so that their sum becomes unity for easier comparison with the NMR results and are included in Table 4. The result agrees reasonably well with the result of a previous fluorescence study of motilin at a lower concentration (0.1 mM in 30% HFP and at 35°C by linear interpolation between 20°C and 40°C), where the longer rotational correlation time was 1.2 ns (Backlund et al., 1995). The new fluorescence anisotropy parameters were used to calculate a spectral density function according to Eq. 3, assuming that the order parameter S^2 can be taken as $A_1/(A_1 + A_2)$. The spectral density function obtained from the fluorescence data is shown as the

TABLE 4 Dynamic parameters of the peptide hormone motilin in 30% HFP at 35°C determined using different methods

Model	Data	A_1	τ_1 (ns)	A_2	τ_2 (ns)	A_3	τ_3 (ns)	χ^2
Two-component	SSDM*	0.50	1.7	0.50	0.060			1.54*
	FAD	0.47	1.7	0.53	0.054			1.07
Three-component	SSDM*	0.36	2.1	0.22	0.59	0.42	0.037	0.37*
	FAD	0.33	2.2	0.17	0.42	0.50	0.029	1.00
MF + R_{ex}[†]	SSDM[‡]	0.49	1.5	0.51	0.054			1.33[‡]
MF + r_{eff}[§]	SSDM[‡]	0.61	1.9	0.39	0.29			2.42[‡]
MF + r_{eff}[§]	SSDM*	0.62	1.9	0.38	0.28			0.62*

The models are two-component (Eqs. 3 and 4) and three-component (Eqs. 10 and 9) models used to fit to NMR and fluorescence results, respectively, as described in the text. MF refers to the two-component model-free approach (Eq. 3), where A_1 corresponds to S^2 and τ_1 and τ_2 correspond to τ_M and τ_{eff}, respectively. The sum of the amplitudes is unity.

*$J(0)$ was estimated as the average of the values from each field strength, and the uncertainty was estimated from the standard deviation of the four values as described in the text.

[†]The coefficient of proportionality for the exchange contribution to the transverse relaxation, ϕ_{ex} was fitted to 8.3×10^{-19} s rad^{-1}, which corresponds to an exchange contribution, R_{ex}, of 0.7 s^{-1} at 14.1 T (600-MHz proton frequency).

[‡]The four $J(0)$ estimates were used with uncertainty estimates propagated from the uncertainty estimates of the relaxation rates.

[§]The effective internuclear distance r_{eff} between the carbon and hydrogen nuclei was estimated as 1.16 Å, which indicates fast motions of considerable amplitude.

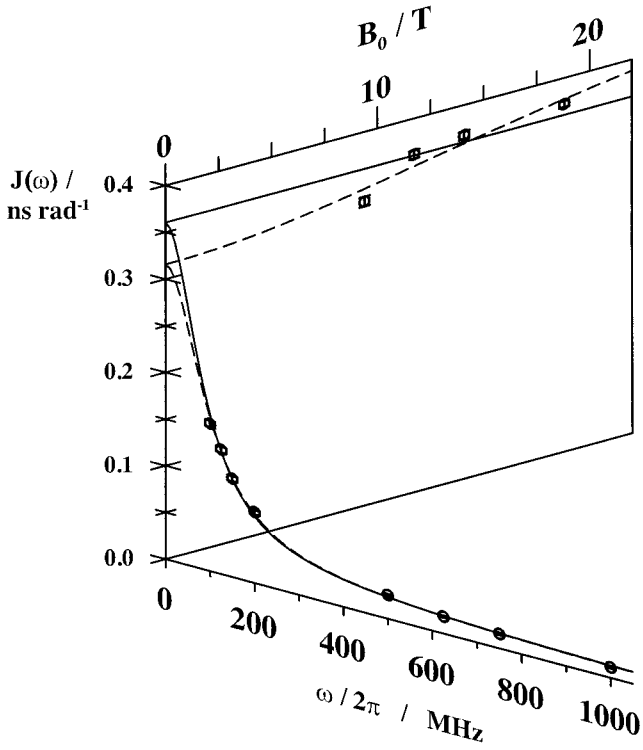

FIGURE 5 Probing the existence of conformational exchange contributions to the transverse auto-relaxation and, consequently, $J(0)^{apparent}$. Two graphs on planes at an angle with one another are shown together to indicate that they have a common intercept. The $J(0)^{apparent}$ as a function of B is shown in the plane directed inwards and the $J(\omega)$ as a function of $\omega/2\pi$ in the plane directed outwards. The solid curves represent the model-free approach when the conformational exchange is assumed to be negligible; i.e., $\phi = 0$. The dashed curves represent the model-free approach when contributions from fast conformational exchange is treated as an adjustable parameter.

dashed curve in Fig. 4 *A*, and the corresponding parameters are included in Table 4. Evidently, the spectral density curve and the corresponding parameters agree very well with the data obtained from NMR on the same system.

More complex dynamic models

The six parameters of a three-component model (Eq. 9) were fitted to the FAD data:

$$C(t) = \sum A_i \exp(-t/\tau_i) \tag{9}$$

The best-fitting values are $A_1 = 0.10$, $\tau_1 = 2.2$ ns, $A_2 = 0.050$, $\tau_2 = 0.42$ ns, $A_3 = 0.15$, and $\tau_3 = 0.029$ ns. Also for this model the sum of the amplitudes is less than the theoretical value of 2/5. The amplitudes were rescaled so that their sum becomes unity. The result is included in Table 4. The small bulge visible in the residuals at the beginning of the curve when fitting the two-component model to the FAD data (Fig. 6) disappears when the three-component model is used.

A careful inspection of the fit of the model-free spectral density function to the SSDM data points (Fig. 4 *A*) reveals certain deviations between the model and the data. The spectral density function corresponding to a three-component model (Eq. 10) was fitted to the spectral density data points:

$$J(\omega) = \frac{2}{5} \sum_{i=1}^{3} \frac{A_i \tau_i}{1 + (\omega \tau_i)^2} \tag{10}$$

The sum of the amplitudes was scaled to be unity. The results are shown in Figs. 4 *B* and 5 and in Table 4. This three-component model is analogous to the three-step model of Clore et al. (1990), but the parameters of the above three-component model (Eq. 10) were used for easier com-

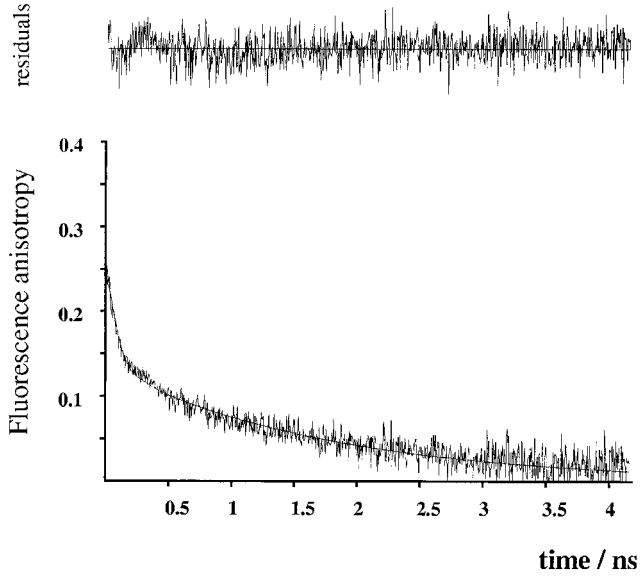

FIGURE 6 FAD of the side chain of Tyr^7 in 5 mM motilin at 35°C in 30% (v/v) HFP. Experimental data and a fitted two-component curve are shown. The residuals show the weighted differences between experimentally determined $I_{\parallel} - I_{\perp}$ and the values obtained for the fitted model as described previously (Kawato et al., 1977; Kouyama et al., 1989). The two-component model had the parameters shown in Table 4. The fluorescence lifetimes were evaluated from the isotropic fluorescence decay ($I_{\parallel} + 2I_{\perp}$) and were as follows: $F_1 = 0.00292$, $\varphi_1 = 4.03$ ns; $F_2 = 0.0123$, $\varphi_2 = 1.33$ ns; and $F_3 = 0.00439$, $\varphi_3 = 0.28$ ns. Data acquisition started before the laser pulse, and the zero time point was determined during fitting.

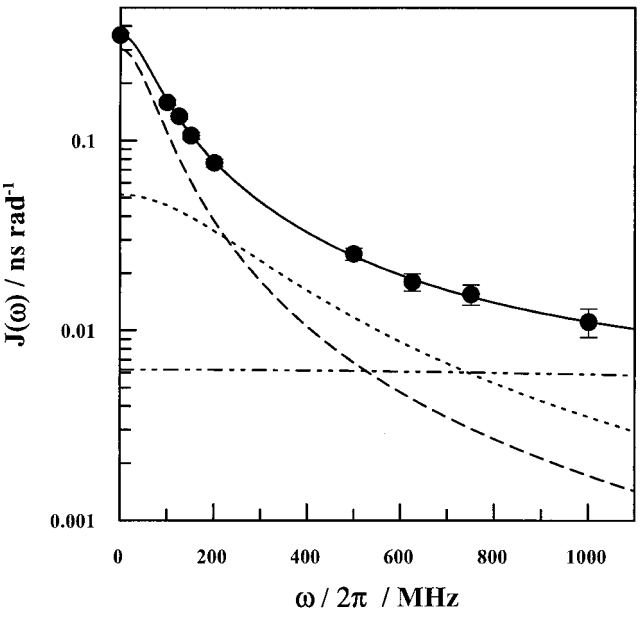

FIGURE 7 The three-component model is shown together with the SSDM data. The sum of the components is shown as the solid curve and the individual components as dashed curves. It is clear that the fastest component is effectively constant over the accessible frequency range.

parison with the FAD results. The three components are shown in Fig. 7. One can see that the fastest component is very close to constant over the entire frequency range studied. This implies that the time constant, and the amplitude of this component should be considered as effective parameters only, and assigning a specific physical meaning to them should only be done with great caution. If the term corresponding to the fastest motions in Eq. 10 makes a negligible contribution to the spectral densities at all frequencies within the studied range, this term can be omitted when fitting to SDM data. The resulting spectral density function resembles the model-free spectral density function, if one would allow the sum of the two remaining amplitudes to take values less than unity. An equivalent expression would be obtained if the internuclear distance were allowed to vary:

$$J(\omega) = \frac{2}{5}\left(\frac{1.09}{r_{\mathrm{eff}}}\right)^6\left(\frac{S^2\tau_{\mathrm{M}}}{1 + (\omega\tau_{\mathrm{M}})^2} + \frac{(1 - S^2)\tau_{\mathrm{e}}}{1 + (\omega\tau_{\mathrm{e}})^2}\right) \quad (11)$$

Here S^2 and $(1 - S^2)$ correspond to A_1 and A_2 in Table 4, respectively. The results from fitting the parameters of Eq. 11 to the SSDM data are also shown in Table 4. A best-fitting internuclear distance of 1.16 Å was obtained. This long distance corresponds to fast internal motions of considerable amplitude, probably including also librations of the tyrosine ring relative to the molecular frame, for example, fluctuations of the χ^2 angle. Furthermore, when using a variable internuclear distance with a large fitted value, the order parameter, the global rotational correlation time, and the effective internal correlation time all increase compared with the results obtained when using a fixed internuclear distance of 1.09 Å (Table 4).

DISCUSSION

SDM is a consistent method to analyze the dynamics of a molecule. As a first step the experimental rates are converted to spectral densities, which allows a check of the consistency of the measured rates. It was at this stage that the inconsistencies of the transverse anti-phase rates were discovered. Taking the anti-phase rate at face value, it gave rise to negative $J(\omega_{\mathrm{H}})$ values, and the effect on $J(0)$ was to increase it significantly. With the SSDM, where the transverse anti-phase rate was omitted, all used rates were consistent and gave a very precise picture of the spectral densities representative of the ^{13}C-H vectors in ϵ-position in the tyrosine ring.

The results of the SSDM could be fitted to a three-parameter dynamic model by the model-free approach to allow comparison with the fluorescence results. Care was taken to ensure that NMR and fluorescence measurements were made on identical samples. One question about the comparison of the two methods is related to the fact that in the FAD experiment the rotational correlation function of the excitation dipole of the excited state is studied, whereas the NMR experiments are sensitive to the dynamical prop-

erties of the electronic ground state. Recent theoretical calculations (Kushwaha and Mishra, 2000) indicate that the geometries of the ground state and the lowest singlet state are similar, i.e., with only a 0.02-Å shortening of the carbon-oxygen distance and a 0.025-Å lengthening of the C^{γ}-C^{δ} bonds upon excitation. The changes outside the aromatic ring are even smaller, indicating that the effect does not spread to the other parts of the polypeptide. It therefore seems reasonable to assume that the dynamic parameters are very similar for the ground and excited states of the aromatic ring.

When the tyrosine residue is excited from the ground state to the lowest-lying singlet state, i.e., the transition relevant to this case, some electron density moves from the γ-carbon, the ζ-carbon, and the hydroxyl oxygen to the δ- and ϵ-carbons (Smolyar and Wong, 1999). This redistribution of electrons is in agreement with a transition moment in the plane of the ring, orthogonal to the symmetry axis (Hooker and Schellman, 1970) (see Fig. 2). One should note that the environment of the aromatic ring is not symmetric, a reason that the symmetry arguments might not be strictly valid. The small changes of the properties of the aromatic ring might lead to small changes in the energy landscape and consequently the dynamic behavior. The experimental data indicate that these effects are not significant in the case of the tyrosine residue in motilin, however.

The comparison of the calculated spectral density curves obtained from NMR relaxation and fluorescence results, which are shown in Fig. 4 *A* with corresponding parameters in Table 4, indicate that the two methods give very similar results in terms of dynamic parameters. The closely coinciding values of S^2 and τ_m give credibility to these parameters, whether they are obtained by FAD or NMR.

Also for the more complex three-component model (Eqs. 10 and 11), a close agreement between the parameters estimated from the FAD and SSDM results is obtained (Fig. 4 *B*; Table 4). A different problem arises when the validity of the dynamic models in the present case is questioned. Our old results from NMR relaxation were measured under almost identical conditions but with the ^{13}C label instead placed on the C^{α} of Leu^{10}. A direct comparison (Table 3) of the spectral densities evaluated at three different magnetic fields in that study, and those found here, shows that with the Leu^{10} label, $J(0)$ was determined to be $\sim$1.0 ns rad^{-1}, whereas 0.3–0.4 ns rad^{-1} was determined here for $J(0)$. The spectral densities at higher frequencies are more similar in the two measurements. The difference in $J(0)$ causes the rather big difference in evaluated overall rotational correlation times (τ_M = 3.1 ns for the Leu^{10}-labeled sample, which should be compared with the value of 1.7 ns according to the fit here of the model-free spectral density function). The striking deviation between the two values might be because of different sample conditions as indicated from preliminary translational diffusion measurements, where $D_t = 1.2\ 10^{-10}$ m^2/s for the sample labeled in the tyrosine side chain and $D_t = 0.7\ 10^{-10}$ m^2/s for the sample labeled in Leu^{10} (data not shown).

If conformational exchange is included in the dynamic model, more parameters are allowed and the fit to the experimental spectral densities is improved (Fig. 6). The agreement between the fluorescence and NMR results remains about the same (Table 4). The statistical evidence for the inclusion of an exchange term is weak. Comparing with the data from the Leu^{10}-labeled peptide, we observe that in that case the $J(0)$ value varies much less with the magnetic field and not in a monotonous manner as in the present case (cf. Table 3, this work, and Table 2 in Jarvet et al., 1996). Therefore, we conclude that the present result shows at least one remaining possible systematic error, the uncertainty of whether the exchange should be considered or not. The variation in the dynamic parameters indicates the uncertainty associated with this error.

Another source of a systematic error is the question of the internuclear C-H distance r_{CH}. We have used the standard value 1.09 Å for evaluation of the spectral densities (Table 3). When the internuclear distance was treated as an adjustable parameter in the model-free spectral density function a best-fitting value of 1.16 Å was obtained. This result is compatible with earlier reports stating that increased internuclear distances give better fits to NMR results (Llinas et al., 1977; Dill and Allerhand, 1979). It is also compatible with the estimates of the internuclear distances by solid-state NMR. Recently, effective distances of 1.12 $\pm$ 0.02 and 1.15 $\pm$ 0.05 Å were reported for the nonequivalent ϵ carbon-proton pairs of L-tyrosine-HCl (De Paul et al., 2000). The effects of increasing the assumed internuclear distance on the model-free parameters are increasing, in particular the internal correlation time and the order parameter, but also to a lesser degree the rotational correlation time (Table 4). This is a second indication of how a systematic error may influence the dynamic parameters. The presently available NMR instrumentation is not sufficient to cover the large frequency range that would be needed to determine the r_{CH} parameter accurately. The fastest component found using the three-component model makes a nonnegligible contribution to the spectral density at the highest frequency (Fig. 7). This raises the question of the validity of Eq. 11 in this particular case.

The estimated values of the correlation time for local motion, τ_e (Table 4), should also be commented on. In the FAD evaluation using the two-component fit, this parameter (then called τ_2) describes an average of all the rapid processes that can be measured. The observation that the sum of the two amplitudes is less than 0.4 is partly because the excitation and emission dipole vectors do not coincide, but could also suggest that there are even more rapid processes occurring, which are not accounted for by the two exponentials. In NMR, the τ_e parameter is not measured accurately in the experiments available with present-day magnets. The highest frequency where the spectral density is evaluated in the present study is 1000 MHz (the sum of the carbon and proton frequencies at an 18-T magnetic field), corresponding to a correlation time of $1/2\pi \times 10^{-9}$ s, i.e., on the order

of 200 ps. There is obviously no real information about processes with faster motions than this to be obtained from NMR relaxation measurements using spectrometers with 800-MHz or lower proton frequencies; i.e., these processes can be treated only with one average or effective parameter.

In the three-component model, two of the time constants fall within the frequency range accessible by SDM (Fig. 7). The fastest component represents fast dynamics of considerable amplitude. Several physical models can account for the observed results. One example of a model compatible with the experimental results is to associate the slowest component with overall tumbling. The intermediate component may be associated with transitions between different rotameric states of the tyrosine side chain, involving the dihedral angles χ_1 and χ_2, which should occur on the sub-nanosecond time scale. The fastest component could then be associated with wobbling motions of the C-H bond vector of considerable amplitude. The types of motion associated with the intermediate and fast components have been observed for a surface-exposed tyrosine residue in a molecular dynamics simulation of glutaredoxin in explicit water (L. Nilsson, Karolinska Institutet, Stockholm, personal communication) and for phenylalanine side chains in antamanide in Langevin dynamic simulations (Bremi et al., 1997).

Some clues to the reasons for the previously observed discrepancies between fluorescence and NMR results can be found by examining the comparable literature data of Table 1. By using the Stokes-Einstein relation one can calculate the hydrodynamic volume compatible with a certain rotational correlation time. We used the temperature-dependent viscosities of water and D_2O. Also the small viscosity increase from the 5% or 10% D_2O used for magnetic field locking in the NMR relaxation studies was accounted for.

Table 1 shows that in nine cases, i.e., Ca^{2+} and apo calbindin D_{9k}, defunct domain of calcium vector protein, Δ^5-3-ketosteroid isomerase, azurin, carp parvalbumin, staphylococcal nuclease, ribonuclease T1 (one of the two entries), and the random coil form of mellitin, there is reasonable to excellent agreement between the results of the two methods. For the other eight entries, i.e., the tetramer of mellitin, motilin, protein G, lysozyme, reduced thioredoxin, oxidized thioredoxin, barstar, ribonuclease T1 (one of the two entries), and the zinc finger Xfin-31, the hydrodynamic volume estimated by the fluorescence method is smaller than the corresponding volume estimated from NMR relaxation data. There is no case where the volume estimated from NMR data is significantly smaller than the corresponding volume estimated from FAD data.

The experimentally estimated hydrodynamic volumes are also compared with volumes calculated from the molecular weight, assuming a spherical shape and protein density of 1.33 g/cm^3 with a 2.8-Å hydration layer (Table 1). Fig. 8 illustrates the correlation between the hydrodynamic volumes calculated from the molecular weight and those calculated from the experimental correlation times from NMR and fluorescence for monomeric, folded proteins (i.e., when excluding the unstructured motilin and mellitin cases and the dimer and tetramer of Δ^5-3 ketosteorid isomerase and mellitin, respectively). Fig. 8 shows that the volumes calculated from the molecular weight, with the assumed monomolecular hydration layer of 2.8 Å, are in reasonably good agreement with the experimental results. In the selected examples the globular proteins are obviously well described by a spherical shape. In many other cases this is not a good approximation, and more complicated models are required. One study has shown an empirical relationship between rotational correlation time and solvent-accessible surface area, thereby accounting for irregular molecular shapes (Krishnan and Cosman, 1998).

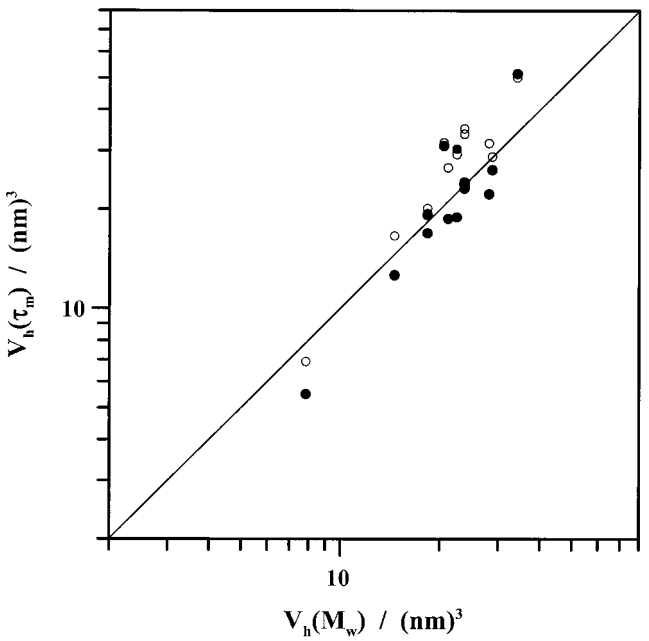

FIGURE 8 Illustrating the correlation between hydrodynamic volumes calculated from a hydrodynamic model and the experimental data for various folded and monomeric proteins, selected from Table 1. The experimental hydrodynamic volumes were evaluated from the FAD data (●) and from the NMR data (○).

A detailed comparison of the experimentally estimated hydrodynamic volumes shown in Fig. 8 shows that there is a clear tendency for the hydrodynamic volume to be overestimated by the NMR method. This is evidenced by a higher average hydrodynamic volume of 27.2 nm^3 for NMR and 22.0 and 23.0 nm^3 for the crude hydrodynamic model and FAD, respectively, when all studies shown in Fig. 8 are taken into account. On average the hydrodynamic volumes estimated from NMR data are 18% larger than the corresponding volumes estimated from FAD data. This indicates that the molecular reorientation is slowed down in the NMR samples. We suggest that this effect is related to the high protein concentrations generally used for the NMR samples. A concentration dependence for the rotational correlation time has indeed been observed, e.g.,

for myoglobin (Iino and Okuda, 1997) and the structural domain of troponin C in complex with the regulatory peptide 1–40 of troponin I (Mercier et al., 2001). Such concentration dependence can be attributed to either specific interactions such as dimerization or nonspecific interactions resulting in heterogeneous aggregates or even a general viscosity effect (Iino and Okuda, 1997). However, from studies on lysozyme it has also been argued that the rotational motions should be independent of the protein concentration (Chirico et al., 1999; Bonincontro et al., 2001).

In the present study, the comparison of careful measurements of molecular dynamics by two different methods, NMR and fluorescence, and the discussion of how parameters may be estimated using different models of motion, show that the methods agree quite satisfactorily in their results and that no obvious systematic errors are associated with either measurement. The present results emphasize that the absolute values of the parameters derived from the models of motion depend more on the choice of model than on the experimental method used to obtain the results. The overall rotational correlation time obtained for motilin in the present study is different when two or three motional components are used to evaluate the results, but fluorescence and NMR results agree in both cases. Another more general consideration is that it is probably beneficial to use motional probes associated with a relatively high generalized order parameter (0.8) to evaluate the global motional parameters with good accuracy. The present case is an example of the situation with a rather mobile probe with a generalized order parameter of ~0.5, which is not ideal for a precise measurement but provides a sensitive comparison between the two experimental methods. The remaining problem of choosing a good model to ascribe a physical meaning to the dynamic parameters is probably the hardest and may require additional information, depending on the system under study. Molecular dynamics simulations may be very useful to suggest realistic dynamic models. Despite these uncertainties, the power of fluorescence and NMR relaxation to report on the dynamics of biological macromolecules in solution is unquestionable.

We thank Britt-Marie Olsson for peptide synthesis and Kalle Kaljuste for help with attaching the t-Boc protecting group on the labeled tyrosine. We acknowledge the Swedish NMR center for the use of their 500- and 800-MHz NMR spectrometers.

This work was supported by a grant from the Swedish Research Council.

REFERENCES

Akke, M., N. J. Skelton, J. Kördel, A. G. Palmer, and W. J. Chazin. 1993. Effects of ion-binding on the backbone dynamics of calbindin-D9k determined by ^{15}N NMR relaxation. *Biochemistry.* 32:9832–9844.

Allard, P., M. Helgstrand, and T. Härd. 1998. The complete homogeneous master equation for a heteronuclear two-spin system in the basis of Cartesian product operators. *J. Magn. Reson.* 134:7–16.

Allard, P., J. Jarvet, A. Ehrenberg, and A. Gräslund. 1995. Mapping of the spectral density function of a C^{α}-H^{α} bond vector from NMR relaxation rates of a ^{13}C-labelled α-carbon in motilin. *J. Biomol. NMR.* 5:133–146.

Backlund, B. M., T. Kulinski, R. Rigler, and A. Gräslund. 1995. Dynamics of the peptide hormone motilin studied by time resolved fluorescence spectroscopy. *Eur. Biophys. J.* 23:407–412.

Bonincontro, A., V. Calandrini, and G. Onori. 2001. Rotational and translational dynamics of lysozyme in water-glycerol solution. *Colloids Surf. B Biointerfaces.* 21:311–316.

Bremi, T., R. Bruschweiler, and R. R. Ernst. 1997. A protocol for the interpretation of side-chain dynamics based on NMR relaxation: application to phenylalanines in antamanide. *J. Am. Chem. Soc.* 119:4272–4284.

Buck, M., J. Boyd, C. Redfield, D. A. MacKenzie, D. J. Jeenes, D. B. Archer, and C. M. Dobson. 1995. Structural determinants of protein dynamics: analysis of ^{15}N NMR relaxation measurements for main-chain and side-chain nuclei of hen egg white lysozyme. *Biochemistry.* 34:4041–4055.

Case, D. A. 1999. Calculations of NMR dipolar coupling strengths in model peptides. *J. Biomol. NMR.* 15:95–102.

Chen, L. X. Q., J. W. Longworth, and G. R. Fleming. 1987. Picosecond time-resolved fluorescence of ribonuclease-T1: a pH and substrate-analog binding study. *Biophys. J.* 51:865–873.

Chirico, G., S. Beretta, and G. Baldini. 1999. Conformation of interacting lysozyme by polarized and depolarized light scattering. *J. Chem. Phys.* 110:2297–2304.

Clore, G. M., A. Szabo, A. Bax, L. E. Kay, P. C. Driscoll, and A. M. Gronenborn. 1990. Deviations from the simple 2-parameter model-free approach to the interpretation of N-15 nuclear magnetic-relaxation of proteins. *J. Am. Chem. Soc.* 112:4989–4991.

Damberg, P., J. Jarvet, P. Allard, and A. Gräslund. 1999. Quantitative estimation of magnitude and orientation of the CSA tensor from field dependence of longitudinal NMR relaxation rates. *J. Biomol. NMR;* 15:27–37.

Damberg, P., J. Jarvet, and A. Gräslund. 2001. Accurate measurement of translational diffusion coefficients: a practical method to account for nonlinear gradients. *J. Magn. Reson.* 148:343–348.

Dayie, K. T., and G. Wagner. 1994. Relaxation-rate measurements for ^{15}N-^{1}H groups with pulsed-field gradients and preservation of coherence pathways. *J. Magn. Reson. Ser. A.* 111:121–126.

De Paul, S. M., K. Saalwächter, R. Graf, and H. W. Spiess. 2000. Sideband patterns from rotor-encoded longitudinal magnetization in MAS recoupling experiments. *J. Magn. Reson.* 146:140–156.

Dill, K., and A. Allerhand. 1979. Small errors in C-H bond lengths may cause large errors in rotational correlation times determined from carbon-13 spin-lattice relaxation measurements. *J. Am. Chem. Soc.* 101:4376–4378.

Farrow, N. A., O. Zhang, A. Szabo, D. A. Torchia, and L. E. Kay. 1995. Spectral density function mapping using ^{15}N relaxation data exclusively. *J. Biomol. NMR.* 6:153–162.

Frey, M. N., T. F. Koetzle, F. Koetzle, M. S. Lehmann, and W. C. Hamilton. 1973. Precision neutron diffraction structure determination of protein and nucleic acid components. X. A comparison between the crystal and molecular structures of L-tyrosine and L-tyrosine hydrochloride. *J. Chem. Phys.* 58:2547–2556.

Frydman, L., G. C. Chingas, Y. K. Lee, P. J. Grandinetti, M. A. Eastman, G. A. Barrall, and A. Pines. 1992. Correlation of isotropic and anisotropic chemical-shifts in solids by 2-dimensional variable-angle-spinning NMR. *Isr. J. Chem.* 32:161–164.

Fushman, D., R. Weisemann, H. Thüring, and H. Rüterjans. 1994. Backbone dynamics of ribonuclease-T1 and its complex with 2′GMP studied by 2-dimensional heteronuclear NMR-spectroscopy. *J. Biomol. NMR.* 4:61–78.

Gibbs, S. J., and C. S. Johnson. 1991. A PFG NMR experiment for accurate diffusion and flow studies in the presence of eddy currents. *J. Magn. Reson.* 93:395–402.

Hooker, T. M. J., and J. A. Schellman. 1970. Optical activity of aromatic chromophores. I. *o*-, *m*-, and *p*-tyrosine. *Biopolymers* 9:1319–1348.

Iino, M., and Y. Okuda. 1997. Concentration dependence of Brownian motion and the viscosity of hemoglobin solutions. *Jpn. J. Appl. Phys.* 36:3786–3790.

Ishima, R., and K. Nagayama. 1995. Protein backbone dynamics revealed by quasi spectral density function analysis of amide N-15 nuclei. *Biochemistry.* 34:3162–3171.

James, D. R. 1985. Fluorescence lifetime quenching and anisotropy studies of ribonuclease T1. *Biochemistry.* 24:5517–5526.

Jarvet, J., P. Allard, A. Ehrenberg, and A. Gräslund. 1996. Spectral-density mapping of $^{13}C^{\alpha}$-$^{1}H^{\alpha}$ vector dynamics using dipolar relaxation rates measured at several magnetic fields. *J. Magn. Reson. B.* 111:23–30.

Kalverda, A. P., M. Ubbink, G. Gilardi, S. S. Wijmenga, A. Crawford, L. J. C. Jeuken, and G. W. Canters. 1999. Backbone dynamics of azurin in solution: slow conformational change associated with deprotonation of histidine 35. *Biochemistry.* 38:12690–12697.

Kawato, S., K. J. Kinosita, and A. Ikegami. 1977. Dynamic structure of lipid bilayers studied by nanosecond fluorescence. *Biochemistry.* 16: 2319–2324.

Kay, L. E., D. A. Torchia, and A. Bax. 1989. Backbone dynamics of proteins as studied by N-15 inverse detected heteronuclear NMR-spectroscopy: application to staphylococcal nuclease. *Biochemistry.* 28: 8972–8979.

Kemple, M. D., P. Buckley, P. Yuan, and F. G. Prendergast. 1997. Main chain and side chain dynamics of peptides in liquid solution from C-13 NMR: melittin as a model peptide. *Biochemistry.* 36:1678–1688.

Kemple, M. D., P. Yuan, K. E. Nollet, J. A. Fuchs, N. Silva, and F. G. Prendergast. 1994. ^{13}C NMR and fluorescence analysis of tryptophan dynamics in wild-type and two single-Trp variants of *Escherichia coli* thioredoxin. *Biophys. J.* 66:2111–2126.

Kördel, J., N. J. Skelton, M. Akke, A. G. Palmer, and W. J. Chazin. 1992. Backbone dynamics of calcium-loaded calbindin-d(9k) studied by 2-dimensional proton-detected N-15 NMR-spectroscopy. *Biochemistry.* 31: 4856–4866.

Kouyama, T., K. Kinosita, and A. Ikegami. 1989. Correlation between internal motion and emission kinetics of tryptophan residues in proteins. *Eur. J. Biochem.* 182:517–521.

Krishnan, V. V., and M. Cosman. 1998. An empirical relationship between rotational correlation time and solvent accessible surface area. *J. Biomol. NMR.* 12:177–182.

Kroes, S. J., G. W. Canters, G. Gilardi, A. van Hoek, and A. J. W. G. Visser. 1998. Time-resolved fluorescence study of azurin variants: conformational heterogeneity and tryptophan mobility. *Biophys. J.* 75: 2441–2450.

Kushwaha, P. S., and P. C. Mishra. 2000. Electronic spectra, excited-state geometries and molecular electrostatic potentials of aromatic amino acids. *J. Photochem. Photobiol.* 137:79–86.

Lipari, G., and A. Szabo. 1982. Model-free approach to the interpretation of nuclear magnetic resonance relaxation in macromolecules. I. Theory and range of validity. *J. Am. Chem. Soc.* 104:4546–4559.

Llinas, M., W. Meier, and K. Wüthrich. 1977. A carbon-13 spin lattice relaxation study of alumichrome at 25.1 MHz and 90.5 MHz. *Biochim. Biophys. Acta.* 492:1–11.

Loria, J. P., M. Rance, and A. G. Palmer. 1999. A relaxation-compensated Carr-Purcell-Meiboom-Gill sequence for characterizing chemical exchange by NMR. *J. Am. Chem. Soc.* 121:2331–2332.

MacKerell, A. D., R. Rigler, L. Nilsson, U. Hahn, and W. Saenger. 1987. Protein dynamics: a time-resolved fluorescence, energetic and molecular-dynamics study of ribonuclease-T_1. *Biophys. Chem.* 26:247–261.

Markley, J. L., A. Bax, Y. Arata, C. W. Hilbers, R. Kaptein, B. D. Sykes, P. E. Wright, and K. Wüthrich. 1998. Recommendations for the presentation of NMR structures of proteins and nucleic acids: IUPAC-IUBMB-IUPAB Inter-Union Task Group on the standardization of data bases of protein and nucleic acid structures determined by NMR spectroscopy. *J. Biomol. NMR.* 12:1–23.

Markus, M. A., K. T. Dayie, P. Matsudaira, and G. Wagner. 1996. Local mobility within villin 14T probed via heteronuclear relaxation measurements and a reduced spectral density mapping. *Biochemistry.* 35: 1722–1732.

Mercier, P., L. Spyracopoulos, and B. D. Sykes. 2001. Structure, dynamics, and thermodynamics of the structural domain of troponin C in complex with the regulatory peptide 1–40 of troponin I. *Biochemistry.* 40: 10063–10077.

Moncrieffe, M. C., N. Juranic, M. D. Kemple, J. D. Potter, S. Macura, and F. G. Prendergast. 2000. Structure-fluorescence correlations in a single tryptophan mutant of carp parvalbumin: solution structure, backbone and side-chain dynamics. *J. Mol. Biol.* 297:147–163.

Nakai, T., J. Ashida, and T. Terao. 1989. Influence of small-amplitude motions on two-dimensional NMR powder patterns: anisotropic vibrations in calcium formate. *Mol. Phys.* 67:839–847.

Nishimoto, E., S. Yamashita, A. G. Szabo, and T. Imoto. 1998. Internal motion of lysozyme studied by time-resolved fluorescence depolarization of tryptophan residues. *Biochemistry.* 37:5599–5607.

Norwood, T. J. 1996. The suppression of cross-relaxation effects in H-1 relaxation measurements. *J. Magn. Reson. Ser. A.* 120:278–283.

Norwood, T. J. 1997. Measurement of the relaxation rates of H-1 longitudinal modes. *J. Magn. Reson.* 125:265–279.

Ottiger, M., and A. Bax. 1998. Determination of relative $N\text{-}H^{N}$, $N\text{-}C'$, $C^{\alpha}\text{-}C'$ and $C^{\alpha}\text{-}H^{\alpha}$ effective bond lengths in a protein by NMR in a dilute liquid crystalline phase. *J. Am. Chem. Soc.* 120:12334–12341.

Palmer, A. G., R. A. Hochstrasser, D. P. Millar, M. Rance, and P. E. Wright. 1993. Characterization of amino acid side chain dynamics in a zinc-finger peptide using C-13 NMR spectroscopy and time-resolved fluorescence spectroscopy. *J. Am. Chem. Soc.* 115:6333–6345.

Palmer, A. G., N. J. Skelton, W. J. Chazin, P. E. Wright, and M. Rance. 1992. Suppression of the effects of cross-correlation between dipolar and anisotropic chemical shift relaxation mechanisms in the measurement of spin spin relaxation rates. *Mol. Phys.* 75:699–711.

Peng, J. W., and G. Wagner. 1992. Mapping of spectral density-functions using heteronuclear NMR relaxation measurements. *J. Magn. Reson.* 98:308–332.

Peng, J. W., and G. Wagner. 1995. Frequency spectrum of NH bonds in eglin c from spectral density mapping at multiple fields. *Biochemistry.* 34:16733–16752.

Rigler, R., F. Claesens, and O. Kristensen. 1985. Picosecond fluorescence spectroscopy in the analysis of structure and motion of bio-polymers. *Anal. Instrum.* 14:525–546.

Rigler, R., J. Roslund, and S. Forsen. 1990. Side-chain mobility in bovine calbindin-d9k: rotational motion of Tyr13. *Eur. J. Biochem.* 188: 541–545.

Sahu, S. C., A. K. Bhuyan, A. Majumdar, and J. B. Udgaonkar. 2000. Backbone dynamics of barstar: a N-15 NMR relaxation study. *Proteins.* 41:460–474.

Seewald, M. J., K. Pichumani, C. Stowell, B. V. Tibbals, L. Regan, and M. J. Stone. 193. 2000. The role of backbone conformational heat capacity in protein stability: temperature dependent dynamics of the B1 domain of streptococcal protein G. *Protein Sci.* 9:1177–1.

Smolyar, A., and C. F. Wong. 1999. Theoretical studies of the spectroscopic properties of tryptamine, tryptophan and tyrosine. *J. Mol. Struct. (Theochem.).* 488:51–67.

Swaminathan, R., N. Periasamy, J. B. Udgaonkar, and G. Krishnamoorthy. 1994. Molten globule-like conformation of barstar: a study by fluorescence dynamics. *J. Phys. Chem.* 98:9270–9278.

Tcherkasskaya, O., J. R. Knutson, S. A. Bowley, M. K. Frank, and A. M. Gronenborn. 2000. Nanosecond dynamics of the single tryptophan reveals multi-state equilibrium unfolding of protein GB1. *Biochemistry.* 39:11216–11226.

Terao, T., H. Miura, and A. Saika. 1986. Dipolar SASS NMR spectroscopy: separation of heteronuclear dipolar powder patterns in rotating solids. *J. Chem. Phys.* 85:3816–3826.

Théret, I., S. Baladi, J. A. Cox, J. Gallay, H. Sakamoto, and C. T. Craescu. 2001. Solution structure and backbone dynamics of the defunct domain of calcium vector protein. *Biochemistry.* 40:13888–13897.

Wong, C. Y., and M. R. Eftink. 1998. Incorporation of tryptophan analogues into staphylococcal nuclease, its V66W mutant, and delta 137–149 fragment: spectroscopic studies. *Biochemistry.* 37:8938–8946.

Wu, P., Y.-K. Li, P. Talalay, and L. Brand. 1994. Characterization of the three tyrosine residues of Δ^5-3-ketosteroid isomerase by time-resolved fluorescence and circular dichroism. *Biochemistry.* 33:7415–7422.

Zhao, Q., C. Abeygunawardana, and A. S. Mildvan. 1996. ^{13}C NMR relaxation studies of backbone and side chain motion of the catalytic tyrosine residue in free and steroid-bound Δ^5–3-ketosteroid isomerase. *Biochemistry.* 35:1525–1532.